LANGMUIR Article
Cite This: Langmuir 2019, 35, 3717−3723
pubs.acs.org/Langmuir

# Simultaneous Silicon Oxide Growth and Electrophoretic Deposition of Graphene Oxide

Pina A. Fritz,*[,†,‡] Stefanie C. Lange,[§] Marcel Giesbers,[∥] Han Zuilhof,[§,⊥] Remko M. Boom,[†] and C. G. P. H. Schroën[†]

[†]Laboratory of Food Process Engineering, Wageningen University, Bornse Weilanden 9, 6708 WG Wageningen, The Netherlands
[‡]School of Chemical and Biomedical Engineering, Nanyang Technological University, 62 Nanyang Drive, 637459, Singapore
[§]Laboratory of Organic Chemistry, Wageningen University, Stippeneng 4, 6708 WE Wageningen, The Netherlands
[∥]Wageningen Electron Microscopy Centre, Wageningen University, Droevendaalsesteeg 1, 6708PB Wageningen, The Netherlands
[⊥]School of Pharmaceutical Science and Technology, Tianjin University, 92 Weijin Road, Tianjin 300072, P. R. China

Supporting Information

**ABSTRACT:** During electrophoretic deposition of graphene oxide (GO) sheets on silicon substrates, not only deposition but also simultaneous anodic oxidation of the silicon substrate takes place, leading to a three-layered material. Scanning electron microscopy images reveal the presence of GO sheets on the silicon substrate, and this is also confirmed by X-ray photoelectron spectroscopy (XPS), albeit that the carbon portion increases with increasing emission angle, hinting at a thin carbon layer. With increasing applied potential and increasing conductivity of the GO solution, the carbon signal decreases, whereas the overall thickness of the added layer formed on top of the silicon substrate increases. Through XPS spectra in which the Si 2p peaks shifted under those conditions to 103−104 eV, we were able to conclude that significant amounts of oxygen are present, indicative of the formation of an oxide layer. This leads us to conclude that GO can be deposited using electrophoretic deposition, but that at the same time, silicon is oxidized, which may overshadow effects previously assigned to GO deposition.

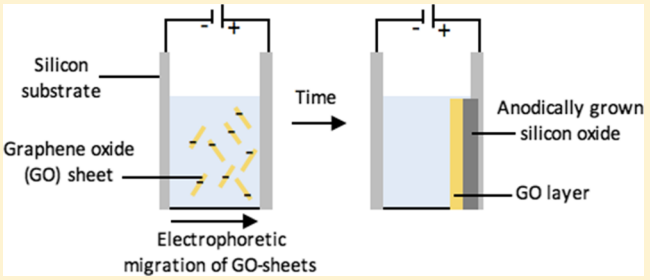


## INTRODUCTION

Transparent electrodes are used in many electronic devices, such as touch screens,[1] thin-film photovoltaics,[2] and transistors.[3] Reduced graphene oxide (GO) thin films are promising cheaper alternatives[4,5] to the current standard indium-doped tin oxide. GO is a 2D material synthesized by chemical exfoliation of graphite,[6] that in its original state shows low conductivity, but when reduced by either thermal,[7] chemical,[8] or electrochemical methods,[9−11] the conductivity can become as high as 100 S/cm.[12] Furthermore, their thermal stability, flexibility, and light transmittance of 80−85% at a wavelength of 550 nm make reduced GO thin films interesting candidates for flexible transparent electrodes.[13−16]

Many techniques to produce GO thin films have been proposed, such as spray-coating,[15,17] spin-coating,[18,19] and electrophoretic deposition.[20−23] When applying the latter technique, GO sheets migrate along an electric field toward the anode because of the negatively charged oxygen groups (typically carboxyl and hydroxyl groups) present on the lateral plane and edges of the GO sheets. Once they reach the surface of the anode, the charged sheets deposit and form a new layer on the electrode, and further reduction can take place.[20] This technique can be applied to many conductive substrates, such as copper, nickel, aluminum, and stainless steel, and is not limited to planar shapes.[20,24−27] A significant advantage of electrophoretic deposition is, thus, that GO is directly reduced during the deposition process.[22]

Apart from the metallic substrates mentioned above, silicon has also been used as the substrate for electrophoretic deposition of GO[21−23] with, for example, the aim to reduce wear and tear in micro- and nanoelectromechanical systems (MEMS/NEMS). This use of GO has led to an order of magnitude reduction in both friction and wear volume, as compared to bare silicon, making GO a promising solid lubricant. For this purpose, layer thicknesses of up to 402 nm have been reported,[21] based primarily on ellipsometry and cross-sectional scanning electron microscopy (SEM) images. In these estimates, the deposited GO layer has, however, to the best of our knowledge, never been distinguished from any anodically oxidized silicon layer underneath. To properly evaluate and understand the performance of the layer, a compositional analysis is, of course, required.

The anodic oxidation of silicon at the interface of an electrolyte has been described with the following reactions.[28]

Received: September 14, 2018
Revised: January 9, 2019
Published: February 20, 2019

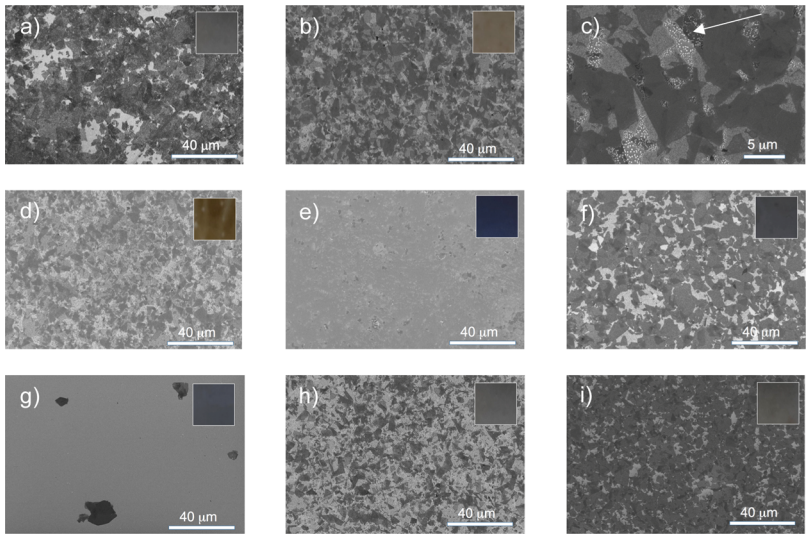


**Figure 1.** SEM images of samples coated for 60 min at 5 (a), 20 (b,c), 30 (d), and 60 V (e) with a solution conductivity of 7 $\mu$S/cm; 60 min at 20 V with a solution conductivity of 16 (f) and 485 $\mu$S/cm (g); and 7 $\mu$S/cm for 30 (h) and 120 (i) min (magnification: 2000×, except b, which is 10 000×). Arrow in c indicates $MnO_2$ crystals.

$$Si + H_2O + h \rightarrow SiOH + H^+ \quad (1)$$

$$2SiOH \rightarrow Si_2O + H_2O \quad (2)$$

$$2Si_2O \rightarrow SiO_2 + 3Si \quad (3)$$

The majority of the oxygen atoms in an anodically grown oxide layer originate from water that is present at or is generated by redox reactions of salt or solvent molecules at the electrode interface. Water only enters the outermost layer, where proton loss occurs, which leads to hydroxyl or oxide ions traveling further into the silicon structure along the electric field.[28] In this paper, we describe the influence of several electrophoretic deposition parameters on the deposition of GO and growth of anodic silicon oxide, using SEM, X-ray photoelectron spectroscopy (XPS), ellipsometry, and color analysis.

## MATERIALS AND METHODS

**Electrophoretic Deposition of GO.** Prior to the coating process, the GO solution (Sigma-Aldrich, 4 mg/mL) with a conductivity of 7 $\mu$S/cm was sonicated and depleted of oxygen using a $N_2$ purge for 30 min. The silicon substrates (1 × 4 cm) were cleaned with Piranha acid (3:1) for 15 min. Later, two silicon substrates were immersed into the deposition cell at a distance of 10 mm, and a constant potential of 5, 20, 30, or 60 V was applied for 1 h (Power supply EPS 1001, Amersham Pharmacia Biotech, USA). To increase the conductivity of the GO solution, 10 or 1000 mM sodium sulfate was added to reach conductivities of 16 and 485 $\mu$S/cm, respectively. After 1 h, silicon substrates were also coated for 0.5 and 2 h at 20 V. As blanks, a silicon substrate was immersed in the GO solution for 1 h without applying a potential, and another silicon substrate was exposed to a sodium sulfate solution with a conductivity of 7 $\mu$S/cm but without any GO present, while applying a potential of 20 V for 1 h.

As GO solutions can vary in sheet size, oxidation degree, and conductivity, as comparison another GO solution (GO(2)) was synthesized from graphite powder (Sigma-Aldrich, <20 $\mu$m) by a modified Hummers method.[29] The resulting GO solution (1 mg/mL) with a conductivity of 14 $\mu$S/cm had a zeta potential of −32.5 mV (Zetasizer Nano-ZS, Malvern instruments, UK), and the d-spacing of the freeze-dried sample (FreeZone 2.5 Plus, Labconco, USA) was measured to be 8.62 Å using X-ray diffraction spectroscopy (D8 Advanced, Bruker, USA). The silicon substrates were coated as described above at 30 V for 1 h. All samples were produced in triplicate.

**Spin Coating of Si Substrates.** The GO(2) solution was sonicated for 30 min, and the silicon substrate (1 × 4 cm) was cleaned with Piranha acid (3:1) for 15 min and etched with 3.5% HF for 4 min. Subsequently, 750 mL GO solution was put onto the substrate for 1 min and spun at 600 rpm for 2 min and 2000 rpm for 1 min. As comparison, the same procedure was conducted without HF etching. All samples were produced in triplicate.

**Preparation of Reference Silicon Substrates.** A silicon substrate (1 × 4 cm) was first cleaned for 15 min in Piranha acid and subsequently etched with 3.5% HF for 4 min to remove oxygen. Another silicon wafer was heated to 1000 °C for 1 h in a lab furnace (Thermo Fischer Scientific) to achieve a thermally grown oxide layer on the outside of the substrate. All samples were produced in triplicate.

**Surface Characterization.** The overall thickness of anodic silicon oxide and GO was characterized at three different positions on each sample (triplicate) using static angle ellipsometry at a wavelength of 632.8 nm and an incidence angle of 70° (SE400, Sentech, Germany). Both the overall layer thickness and the refractive index were used as fitting parameters and average values with standard deviations were calculated accordingly. Static (80°) and angle-resolved (0°−80° between the sample and detector) X-ray photoelectron spectra were measured (XPS, JPS-900 JEOL, Japan) to evaluate the chemical composition of each surface. The element concentrations on the surfaces of the individual sample sets were averaged and the standard deviations were calculated accordingly. SEM images of the top surface (2000 and 10 000×) and the cross section (350 000×) were taken using 2 kV acceleration voltage (SEM, Magellan 400, FEI, USA). Atomic force microscopy (AFM) surface topography images were acquired by an Asylum Research MFP-3D SA AFM (Oxford Instruments, United Kingdom). A sharp knife was used to scratch the surfaces. The scratched surfaces were rinsed with water.

## RESULTS AND DISCUSSION

During electrophoretic deposition, GO sheets migrated toward the positively charged electrode (anode) and deposited on the silicon substrate. After the coating process, the resulting modified substrates had different colors depending on the process potential, solution conductivity, and coating time used, varying between brownish, grey, and blue (Figure 1, inserts).



DOI: 10.1021/acs.langmuir.8b03139
Langmuir 2019, 35, 3717−3723

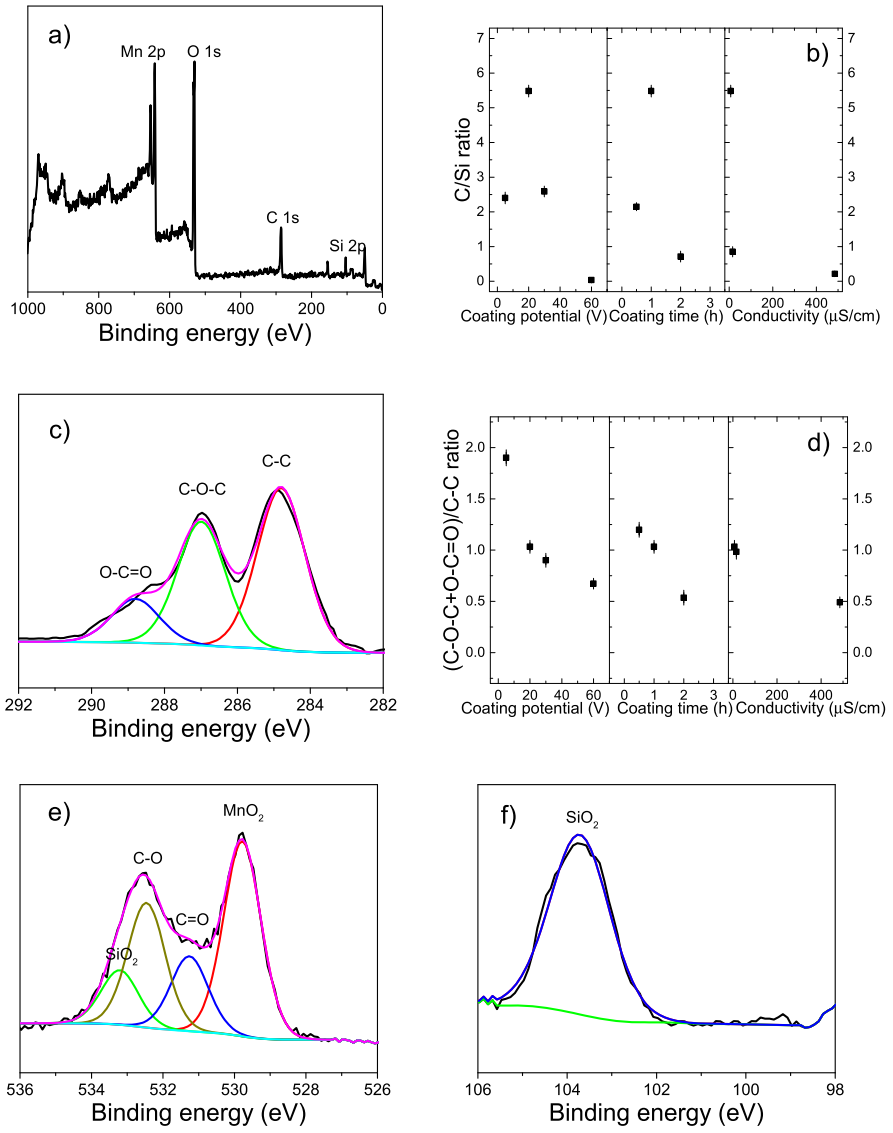


**Figure 2.** (a) XPS wide scan of a sample coated at 20 V for 1 h at 7 $\mu$S/cm. (b) Ratio of C/Si from XPS wide scans of samples coated at various potentials, coating times, and solution conductivities (standard deviations are <10%) (c) C 1s XPS narrow scan of a sample coated at 20 V for 1 h at 7 $\mu$S/cm. (d) Ratio of O-bound carbon atoms versus C-bound carbon atoms (standard deviations are <10%). The value of the original GO sample is indicated in the *Y*-axis. O 1s (e) and Si 2p (f) XPS narrow scan of a sample coated at 20 V for 1 h at 7 $\mu$S/cm.

In literature, these colors were directly related to GO thickness and were implied to correlate with a deposition of hundreds of nanometers of GO.[21] The SEM images in Figures 1 and S1, however, reveal sharp contours of individual GO sheets and the visibility of the underlying substrate is first decreasing while going from 5 to 20 V and then increasing with further increasing coating potential (Figure 1a–e; see also Figure S1a,b in the Supporting Information), conductivity of the GO solution (Figure 1f,g; see also Figure S1c,d), and coating time (Figure 1h,i; see also Figure S1e,f). For example, on the sample coated at 60 V, only a few individual sheets can be found (Figure S1b), thus the blue color of the surface is most likely not caused by the deposited GO but expected to be related to an anodically grown silicon oxide layer.[30]

The presence of silicon oxide was confirmed using XPS analysis. In all samples, a silicon, oxygen, and carbon peak can be detected (Figures 2a and S2). Although native silicon has a Si 2p peak at 99 eV (Figure 3d,e, bottom), the silicon peaks of the GO-coated silicon samples are between 103 and 104 eV (Figures 2f and S5). This is comparable to the Si 2p peak position of a thermally oxidized silicon substrate (Figure 3d,e, top) and of a sample exposed to a sodium sulfate solution for 1 h while applying 20 V (Figure S9). As a reference, GO sheets can also be spin coated onto an etched silicon substrate, but in this case the Si 2p position stays at 99 eV because no silicon oxidation occurs during the process (Figure S8).

The high O/C ratio of 1.6 in the XPS wide scan of the sample coated at 20 V for 1 h (Figure 2a) reveals the presence of more oxygen-containing species on the surface next to GO that has an O/C ratio of 0.4 (Figure 3a). The O 1s narrow scan of GO (Figure 3c) can be fitted with two peaks related to carbonyl and carboxyl groups on the GO sheets, whereas the O 1s narrow scans of the GO-coated Si-substrates reflect the additional presence of $SiO_2$ and $MnO_2$ (Figure 2e and S4). The appearance of the manganese peak can be traced back to the potassium permanganate customarily used during liquid synthesis of GO. During the electrophoretic coating process, $MnO_2$ can be formed, leading to the deposition of $MnO_2$



DOI: 10.1021/acs.langmuir.8b03139
*Langmuir* 2019, 35, 3717–3723

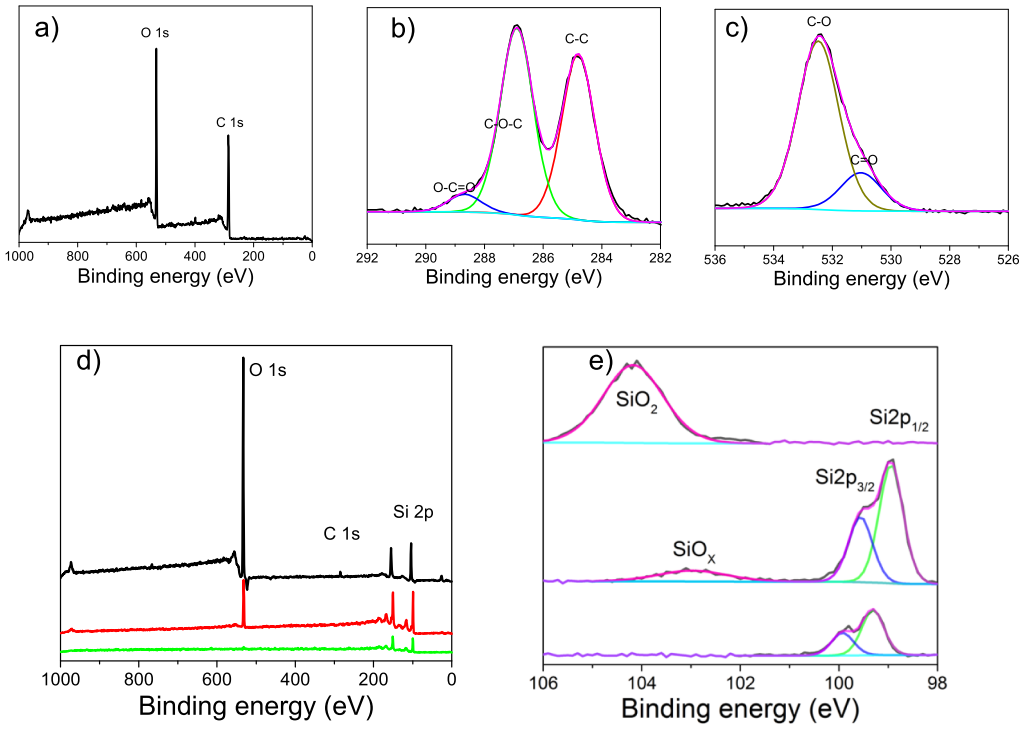


**Figure 3.** (a) XPS wide scan, (b) C 1s narrow scan, and (c) O 1s narrow scan of GO. (d) XPS wide scan and (e) narrow scan of HF-etched silicon substrate (bottom), silicon substrate exposed to $O_2$ (middle), and thermally oxidized silicon substrate (top).

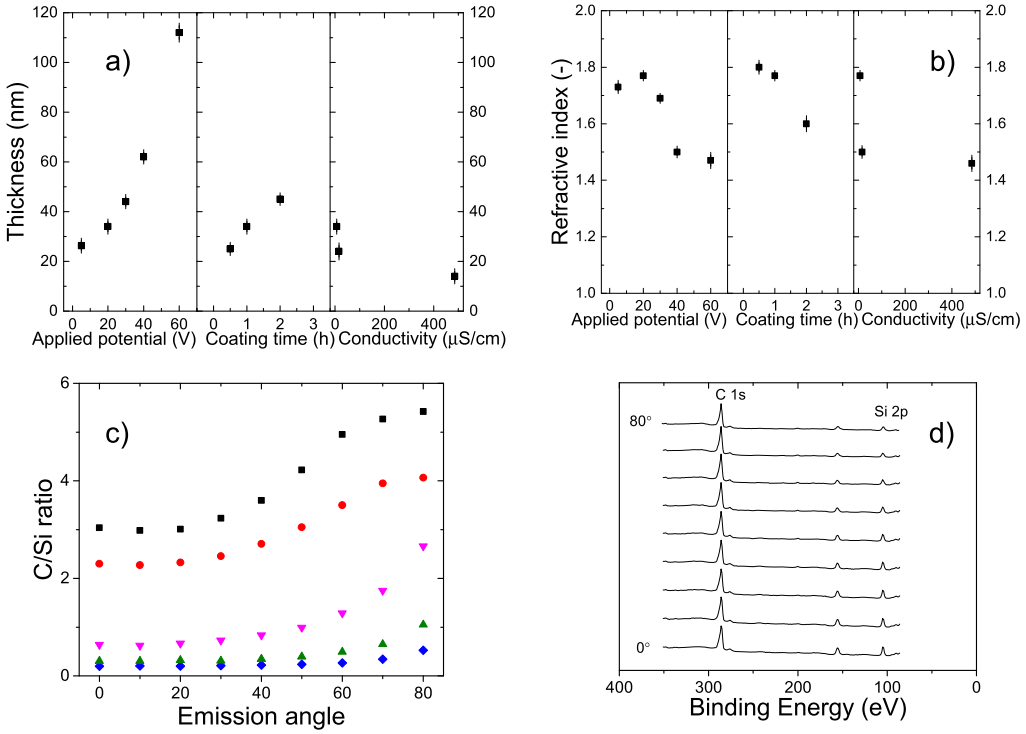


**Figure 4.** (a) Overall layer thickness (Si oxide and GO) and (b) overall refractive index determined by ellipsometry (standard deviation is <10 and <2%, respectively). (c) Ratio of C vs Si signal over XPS emission angle of samples coated at various potentials, coating times, and solution conductivities. Black square: 20 V, 1 h, at 7 $\mu$S/cm. Red circle: 30 V, for 1 h, at 7 $\mu$S/cm. Purple star: 40 V, 1 h, at 7 $\mu$S/cm. Blue diamond: 60 V, 1 h, at 7 $\mu$S/cm. Pink downward triangle: 20 V, 1 h, at 16 $\mu$S/cm. Green upward triangle: 20 V, 1 h with, at 485 $\mu$S/cm. Cross: 20 V, 0.5 h, at 7 $\mu$S/cm. Star: 20 V, 2 h, at 7 $\mu$S/cm. (d) XPS wide scans at different emission angles of a sample coated at 20 V for 1 h at a solution conductivity of 7 $\mu$S/cm.

nanoparticles (arrow in Figures 1c and S1; see also the spikes in S11). A similar process has been discussed by Yu et al. for the synthesis of graphene/$MnO_2$ nanostructured textiles for improved capacitance in large-scale energy storage systems.[31]



DOI: 10.1021/acs.langmuir.8b03139
*Langmuir* 2019, 35, 3717−3723

Looking at the XPS C 1s narrow scans (Figures 2c and S3) of the coated Si substrates, the ratio of carbon atoms bound to oxygen atoms, for example, in carbonyl or carboxyl groups versus carbon atoms connected with only other carbon atoms, decreases by 12−60% compared to the original ratio in GO, indicating the electrochemical reduction of GO during the electrophoretic deposition process (Figure 2d).[22] Although the detailed mechanism behind this deoxygenation of carboxyl groups on the GO sheets is not the topic of our investigation, two literature-based hypotheses deserve mentioning, namely a Kolbe-like release of $CO_2$ after contact with the electrode, leading to potential crosslinks between different GO sheets,[32,33] or the crosslinking between protic functional groups of GO and Si-containing molecules, such as tetraethyl orthosilicates.[34,35] The samples coated at 30 V with the alternatively prepared GO(2) solution show similar results; the SEM image (Figure S7a) reveals the presence of GO sheets on the surface and an O/C ratio of 5.6, as well as the shift of the Si peak to 103 eV (Figure S7c) indicative of the presence of silicon oxide. The absence of the Mn peak in the XPS spectra of GO(2) can be related to different ion residues in solution, similar to the samples coated with the GO solution containing additional sodium sulfate (Figures S2c,d and S4c,d). This indicates that GO solution characteristics, such as solution conductivity, are of high importance for the coating process and the resulting quality of the deposited layer.

Although no GO deposition and no silicon oxidation can be detected on a silicon substrate simply exposed to the GO solution without applying a potential (Figure S10), the overall thickness (silicon oxide and GO) of the layers formed when coated at 20 V for 1 h was 34 nm, and height differences measured by AFM after applying a scratch in the GO layer (Figure S11) suggest the GO thickness to be around 15 nm. With increasing potential, the overall thickness increased to 112 nm (Figure 4a) but the C/Si ratio decreases as depicted in Figure 2b. The angle-resolved XPS images show a steeper rise of the C/Si ratio over the emission angles with a higher coating potential (Figure 4c), indicating that the carbon layer gets thinner, whereas the position of the Si 2p peak is not changing (Figure 4d). Furthermore, the refractive index shifts from 1.77 to 1.46 (Figure 4b) at a high coating potential, and as such becomes equal to the value of thermally oxidized silicon (1.46). This indicates that with increasing potential, the amount of GO deposition is decreasing, which can be related to an increase in electrolysis of water and bubble formation at the interface, destroying the GO layer.[36,37] Furthermore, owing to the increased current, anodic silicon oxidation is favored.[28] This is supported by the cross-sectional SEM images in Figure 5. On the 20 V sample, the porous GO layer is visible, whereas at 60 V, the layer appears flat and dense, similar to the sample coated with the reference GO(2) solution at 30 V (Figure S7b).

With increasing solution conductivity, both the C 1s XPS peak and the overall thickness of the layers are decreasing, and the refractive index approaches 1.46 (i.e., again reaches the reference value for silicon oxide). This can be related to a stronger screening of the charges on the sheets and, thus, slower particle motion and less GO deposition at higher ionic strength.[38,39] At the same time, as described before also, a higher anion concentration leads to a higher ionic current, which can be related to more extensive surface reactions, such as silicon oxidation[28] and water electrolysis. The latter causes bubble formation, and can thus lead to detachment of GO sheets.[36] A study of the layer composition as a function of time shows that the C 1s peak is first increasing (Figure S2e) as is the overall layer thickness (Figure 4a), which is then followed by a decrease in the carbon signal (Figure S2f) at a continued increase in the overall layer thickness. This together with the decrease in refractive index toward that of silicon oxide (Figure 4b) leads us to conclude that first GO deposition takes place, although the GO thickness is later stagnant or even lost, whereas Si-oxidation becomes the main factor for increasing overall thickness of the formed layer. This means that within one processing step, a three-layered substrate (silicon/silicon oxide/GO) can be produced, and that the thickness of the different layers can be adjusted to some extent, depending on the coating time, coating potential, and the conductivity of the solution.

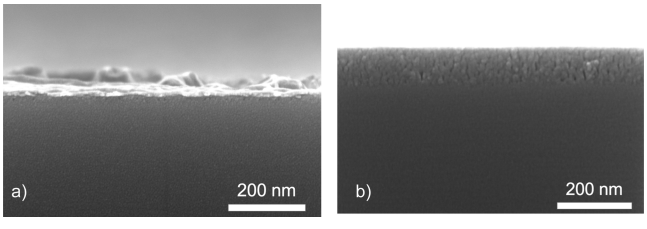


**Figure 5.** Cross-sectional SEM images of samples coated at (a) 20 V and (b) 60 V for 1 h at a solution conductivity of 7 $\mu$S/cm.

## CONCLUSIONS

During the electrophoretic deposition of GO, apart from deposition and anodic reduction of GO, oxidation of the Si substrate also takes place. This anodic oxidation of Si leads to color changes and changes in the overall layer thickness. In literature, these effects were contributed to GO deposition, but here we show via SEM, XPS, and AFM analyses, the complex composition of the formed adlayer, in which both GO and $SiO_x$ appear in amounts and ratios dependent on deposition voltage, solution conductivity, and reaction times. The more detailed analysis of the origin of this adlayer allows a better understanding of the use of GO layers in a wide variety of applications.

## ASSOCIATED CONTENT

### Supporting Information

The Supporting Information is available free of charge on the ACS Publications website at DOI: 10.1021/acs.langmuir.8b03139.

SEM, XPS, and angle-resolved XPS data of different samples and information about the spin-coated samples. (PDF)

## AUTHOR INFORMATION

### Corresponding Author

*E-mail: pina.fritz@wur.nl.

### ORCID

Pina A. Fritz: 0000-0002-4237-9341

Han Zuilhof: 0000-0001-5773-8506

### Notes

The authors declare no competing financial interest.



DOI: 10.1021/acs.langmuir.8b03139
*Langmuir* 2019, 35, 3717−3723

## ■ ACKNOWLEDGMENTS

This work was sponsored by the Institute of Sustainable Process Technology (ISPT) in the Netherlands. Furthermore, we would like to thank Barend van Lagen and Andriy Kuzmyn (Laboratory of Organic Chemistry, Wageningen University), Remco Fokkink (Laboratory of Physical Chemistry and Soft Matter, Wageningen University), and Penghui Zhang (School of Chemical and Biomedical Engineering, Nanyang Technological University) for scientific support.

## ■ REFERENCES

(1) Wang, J.; Liang, M.; Fang, Y.; Qiu, T.; Zhang, J.; Zhi, L. Rod-Coating: Towards Large-Area Fabrication of Uniform Reduced Graphene Oxide Films for Flexible Touch Screens. *Adv. Mater.* **2012**, *24*, 2874−2878.
(2) Yin, Z.; Zhu, J.; He, Q.; Cao, X.; Tan, C.; Chen, H.; Yan, Q.; Zhang, H. Graphene-Based Materials for Solar Cell Applications. *Adv. Energy Mater.* **2014**, *4*, 1−19.
(3) Huang, X.; Zeng, Z.; Fan, Z.; Liu, J.; Zhang, H. Graphene-Based Electrodes. *Adv. Mater.* **2012**, *24*, 5979−6004.
(4) Wöbkenberg, P. H.; Eda, G.; Leem, D.-S.; de Mello, J. C.; Bradley, D. D. C.; Anthopoulos, T. D.; Anthopoulos, T. D. Reduced Graphene Oxide Electrodes for Large Area Organic Electronics. *Adv. Mater.* **2011**, *23*, 1558−1562.
(5) Kumar, S.; Kumar, S.; Srivastava, S.; Yadav, B. K.; Lee, S. H.; Sharma, J. G.; Doval, D. C.; Malhotra, B. D. Reduced Graphene Oxide Modified Smart Conducting Paper for Cancer Biosensor. *Biosens. Bioelectron.* **2015**, *73*, 114−122.
(6) Dreyer, D. R.; Park, S.; Bielawski, C. W.; Ruoff, R. S. The Chemistry of Graphene Oxide. *Chem. Soc. Rev.* **2010**, *39*, 228−240.
(7) Yang, L.; Kong, J.; Yee, W. A.; Liu, W.; Phua, S. L.; Toh, C. L.; Huang, S.; Lu, X. Highly Conductive Graphene by Low-Temperature Thermal Reduction and in Situ Preparation of Conductive Polymer Nanocomposites. *Nanoscale* **2012**, *4*, 4968.
(8) Park, S.; An, J.; Potts, J. R.; Velamakanni, A.; Murali, S.; Ruoff, R. S. Hydrazine-Reduction of Graphite- and Graphene Oxide. *Carbon* **2011**, *49*, 3019−3023.
(9) Shao, Y.; Wang, J.; Engelhard, M.; Wang, C.; Lin, Y. Facile and Controllable Electrochemical Reduction of Graphene Oxide and Its Applications. *J. Mater. Chem.* **2010**, *20*, 743−748.
(10) Zhang, X.; Zhang, D.; Chen, Y.; Sun, X.; Ma, Y. Electrochemical Reduction of Graphene Oxide Films: Preparation, Characterization and Their Electrochemical Properties. *Chin. Sci. Bull.* **2012**, *57*, 3045−3050.
(11) Yu, H.; He, J.; Sun, L.; Tanaka, S.; Fugetsu, B. Influence of the Electrochemical Reduction Process on the Performance of Graphene-Based Capacitors. *Carbon* **2013**, *51*, 94−101.
(12) Gao, W. *Graphene Oxide Reduction Recipes, Spectroscopy, and Applications*; Springer International Publishing AG: Switzerland, 2015.
(13) Gao, K.; Shao, Z.; Wu, X.; Wang, X.; Li, J.; Zhang, Y.; Wang, W.; Wang, F. Cellulose Nanofibers/Reduced Graphene Oxide Flexible Transparent Conductive Paper. *Carbohydr. Polym.* **2013**, *97*, 243−251.
(14) Yin, Z.; Wu, S.; Zhou, X.; Huang, X.; Zhang, Q.; Boey, F.; Zhang, H. Electrochemical Deposition of ZnO Nanorods on Transparent Reduced Graphene Oxide Electrodes for Hybrid Solar Cells. *Small* **2010**, *6*, 307−312.
(15) Pham, V. H.; Cuong, T. V.; Hur, S. H.; Shin, E. W.; Kim, J. S.; Chung, J. S.; Kim, E. J. Fast and Simple Fabrication of a Large Transparent Chemically-Converted Graphene Film by Spray-Coating. *Carbon* **2010**, *48*, 1945−1951.
(16) Karthick, R.; Brindha, M.; Selvaraj, M.; Ramu, S. Stable Colloidal Dispersion of Functionalized Reduced Graphene Oxide in Aqueous Medium for Transparent Conductive Film. *J. Colloid Interface Sci.* **2013**, *406*, 69−74.
(17) Lee, S. C.; Some, S.; Wook Kim, S.; Jun Kim, S.; Seo, J.; Lee, J.; Lee, T.; Ahn, J.-H.; Choi, H.-J.; Chan Jun, S. Efficient Direct Reduction of Graphene Oxide by Silicon Substrate. *Sci. Rep.* **2015**, *5*, 12306.
(18) Watcharotone, S.; Dikin, D. A.; Stankovich, S.; Piner, R.; Jung, I.; Dommett, G. H. B.; Evmenenko, G.; Wu, S.-E.; Chen, S.-F.; Liu, C.-P.; et al. Graphene−Silica Composite Thin Films as Transparent Conductors. *Nano Lett.* **2007**, *7*, 1888−1892.
(19) Becerril, H. A.; Mao, J.; Liu, Z.; Stoltenberg, R. M.; Bao, Z.; Chen, Y. Evaluation of Solution-Processed Reduced Graphene Oxide Films as Transparent Conductors. *ACS Nano* **2008**, *2*, 463−470.
(20) Chavez-Valdez, A.; Shaffer, M. S. P.; Boccaccini, A. R. Applications of Graphene Electrophoretic Deposition. A Review. *J. Phys. Chem. B* **2012**, *117*, 1502−1515.
(21) Liang, H.; Bu, Y.; Zhang, J.; Cao, Z.; Liang, A. Graphene Oxide Film as Solid Lubricant. *ACS Appl. Mater. Interfaces* **2013**, *5*, 6369−6375.
(22) An, S. J.; Zhu, Y.; Lee, S. H.; Stoller, M. D.; Emilsson, T.; Park, S.; Velamakanni, A.; An, J.; Ruoff, R. S. Thin Film Fabrication and Simultaneous Anodic Reduction of Deposited Graphene Oxide Platelets by Electrophoretic Deposition. *J. Phys. Chem. Lett.* **2010**, *1*, 1259−1263.
(23) Ishikawa, R.; Ko, P. J.; Kurokawa, Y.; Konagai, M.; Sandhu, A. Electrophoretic Deposition of High Quality Transparent Conductive Graphene Films on Insulating Glass Substrates. *J. Phys. Conf. Ser.* **2012**, *352*, 012003.
(24) Vlachova, J.; Labuda, J.; Hynek, D.; Zitka, O.; Kizek, R. Utilization of Graphene Oxide Electrophoretic Deposition for Construction of Electrochemical Sensors and Biosensors. *J. Met. Nanotechnologies* **2015**, *3*, 57−63.
(25) Park, J. H.; Park, J. M. Electrophoretic deposition of graphene oxide on mild carbon steel for anti-corrosion application. *Surf. Coat. Technol.* **2014**, *254*, 167−174.
(26) Lake, J. R.; Cheng, A.; Selverston, S. Graphene Metal Oxide Composite Supercapacitor Electrodes. *J. Vac. Sci. Technol. B* **2012**, *30*, 03D118.
(27) Hasan, S. A.; Rigueur, J. L.; Harl, R. R.; Krejci, A. J.; Gonzalo-Juan, I.; Rogers, B. R.; Dickerson, J. H. Transferable Graphene Oxide Films with Tunable Microstructures. *ACS Nano* **2010**, *4*, 7367−7372.
(28) Zhang, X. G. *Electrochemistry of Silicon and Its Oxide*; Kluwer Academic Publishers, 2001.
(29) Wang, J.; Ge, X.; Liu, Z.; Thia, L.; Yan, Y.; Xiao, W.; Wang, X. Heterogeneous Electrocatalyst with Molecular Cobalt Ions Serving as the Center of Active Sites. *J. Am. Chem. Soc.* **2017**, *139*, 1878−1884.
(30) Henrie, J.; Kellis, S.; Schultz, S. M.; Hawkins, A. Electronic Color Charts for Dielectric Films on Silicon. *Opt. Express* **2004**, *12*, 1464−1469.
(31) Yu, G.; Hu, L.; Vosgueritchian, M.; Wang, H.; Xie, X.; McDonough, J. R.; Cui, X.; Cui, Y.; Bao, Z. Solution-Processed Graphene/MnO2nanostructured Textiles for High-Performance Electrochemical Capacitors. *Nano Lett.* **2011**, *11*, 2905−2911.
(32) Vijh, A. K.; Conway, B. E. Electrode Kinetic Aspects of the Kolbe Reaction. *Chem. Rev.* **1967**, *67*, 623−664.
(33) Diba, M.; Fam, D. W. H.; Boccaccini, A. R.; Shaffer, M. S. P. Electrophoretic Deposition of Graphene-Related Materials: A Review of the Fundamentals. *Prog. Mater. Sci.* **2016**, *82*, 83−117.
(34) Kou, L.; Gao, C. Making silicananoparticle-covered graphene oxide nanohybrids as general building blocks for large-area superhydrophilic coatings. *Nanoscale* **2011**, *3*, 519−528.
(35) Liu, Y.; Meng, X.; Liu, Z.; Meng, M.; Jiang, F.; Luo, M.; Ni, L.; Qiu, J.; Liu, F.; Zhong, G. Preparation of a Two-Dimensional Ion-Imprinted Polymer Based on a Graphene Oxide/SiO2 Composite for the Selective Adsorption of Nickel Ions. *Langmuir* **2015**, *31*, 8841−8851.
(36) Chávez-Valdez, A.; Boccaccini, A. R. Innovations in Electrophoretic Deposition: Alternating Current and Pulsed Direct Current Methods. *Electrochim. Acta* **2012**, *65*, 70−89.
(37) Diba, M.; García-Gallastegui, A.; Klupp Taylor, R. N.; Pishbin, F.; Ryan, M. P.; Shaffer, M. S. P.; Boccaccini, A. R. Quantitative Evaluation of Electrophoretic Deposition Kinetics of Graphene Oxide. *Carbon* **2014**, *67*, 656−661.



DOI: 10.1021/acs.langmuir.8b03139
*Langmuir* 2019, 35, 3717−3723

(38) Ferrari, B.; Moreno, R. Electrophoretic Deposition of Aqueous Alumina Slips. *J. Eur. Ceram. Soc.* **1997**, *17*, 549−556.
(39) Besra, L.; Liu, M. A Review on Fundamentals and Applications of Electrophoretic Deposition (EPD). *Prog. Mater. Sci.* **2007**, *52*, 1−61.



DOI: 10.1021/acs.langmuir.8b03139
*Langmuir* 2019, 35, 3717−3723